Interaction of charged magnetic nanoparticles with surfaces

M. A. Valdez[a], J. Juárez[b], J. Ibarra[c] and M. A. Valdés[b]

[a]*Instituto Mexicano del Petróleo, Ciudad de México,*
[b]*Departamento de Física, Universidad de Sonora, Hermosillo, Sonora, México,*
[c]*Unidad Navojoa, Universidad de Sonora, Hermosillo, Sonora, México.*

Received 18 December 2023; accepted 25 April 2024

The behavior of magnetic nanoparticles covering the surface with positive charges (MN), suspended in a continuous medium, was simulated by Brownian dynamics. Then, we studied the behavior of the MN in an aqueous-like suspension and their adsorption on a negatively charged surface, mimicking a mica surface. After several microseconds, particles are deposited onto the charged surface. Experimental results of ordered magnetic nanoparticles in surfaces are compared with the present simulation results of MN in two dimensions. We also demonstrate the effect of charged MN on the hexagonal structure when electrical repulsions dominate against magnetic dipole-dipole and van der Waals attractions. On one hand, the adsorption of MN on the surface depends on the electrostatic attraction force with the surface, while the surface organization of MN results from balancing electrostatic repulsion forces and magnetic attraction forces among particles. In magnetic nanoparticles simulated with a non-charged surface or weakly charged surface, dipole-dipole interactions dominate the particle-particle interactions, and the interactions between particles and a mica-like surface are conducted by van der Waals forces.

Keywords: Magnetic nanoparticles; Brownian dynamics; 2D-arrangement.

DOI: https://doi.org/10.31349/RevMexFis.70.051004

1. Introduction

Magnetic Nanoparticles (MN) have been applied in different fields such as: biomedicine, agriculture, biosensing, environment, and so on [1]. As the magnetic properties of MN depend on their sizer and surface charge distribution, MNs have been tuned by covering their surface with different synthetic and natural polymers, as well as small organic molecules [2], opening a plethora of new application such to capture bacteria from contaminated water [3], and improving the interaction with cancer cells through electrostatic attraction [4], among other. On the other hand, nanoparticles in interfaces show interesting optical, magnetic, and electric properties, including quantum effects [5]. However, the selection and control of the size, charge, magnetic dipole, and morphology are important to achieve desired properties [6]. Two dimensional arrays of MN at solid surfaces have been used for storage information [7,8]. Different experiments have been performed to obtain ordered MN on a solid surface. Lee et. al [9] using Langmuir Blodgett methods obtained ordered MN monolayers covered with an oleate steric acid complex; also, using the same method, Fujimori *et al.* [10] obtained ordered monolayers and multilayers of Fe_3O_4 and $CoFe_2O_4$ covered by stearic acid. Recently, Morga *et al.* [11], performed charged hematite MN monolayers on mica, however they did not obtain ordered nanoparticles, probably due to the small number of electric charges on the hematite MN surface. On the other hand, using a different method to synthesize hematite, Tadic *et al.* [12] obtained ordered MN with an average diameter of 8 nm and covered with oleic acid by Langmuir-Blodgett through. Recently some researchers performed experiments to investigate de deposition process of MN on a solid substrate under the influence of magnetic fields [13]; however, there have been few computational models to analyze the deposition process of nanoparticles on solid surfaces. Kulkarni and Biswas [6], using Brownian Dynamics simulation, investigated de deposition of nanoparticles onto a solid in presence of electric and van der Walls forces. Monte Carlo simulations have been performed to investigate MN in two dimensions to understand the behavior of magnetite covered with oleic acid on carbon sputtered cooper grids [14]. In this work we perform Brownian Dynamics simulations using a model of charged MN to understand the deposition of MN on solid surfaces. We use a similar model used before to investigate the magnetic behavior of red blood cells [15]. Firstly, we introduce the model and the different variables used in simulating the deposition of charged and uncharged MN on a solid surface. Subsequently, we show the applicability of the Brownian dynamic model in simulating the adsorption of MN on the solid surface. Our results demonstrate that electric charge on the MN surface acts as the driving force to achieving an ordered structure of MNs in two-dimensional arrays on both charged and uncharged solid surfaces.

1.1. Brownian dynamics simulation

We perform Brownian dynamics for a system of N charged and magnetic particles in presence of a charged wall, simulating a mica surface in aqueous solution. We use the Langevin equation and the Ermak and McCammon algorithm [15,16]

$$r_i\left(t+\Delta t\right) = r_i(t) + \frac{D_t \Delta t}{K_B T} \times \left(\sum_{j=1}^{N} F_{ij} + F_{ij}^{Y} + F_{i,w}\right) + R_i(\Delta t), \quad (1)$$

where Δt is the time interval , $r_i\,(t)$ is the vector position of the i particle at time t, D_t is the translational diffusion coefficient of particles at very diluted solution, K_B is the Boltzmann constant, T is the absolute temperature, F_{ij} is the magnetic force between the i and the j particles through magnetic dipole interactions, F_{ij}^{Y} is the electrostatic force between particles i and j, q is the electric charge of particles, $F_{i,w}$ is the force of particle i with the charged wall and $R_i(\Delta t)$ is the random vector displacement due to the solvent molecules interaction with particle i, which averages zero displacement and covariance [16].

$$< R_i\,(\Delta t)\,R_j\,(0) \geq 6D_t\Delta t\delta_{ij}, \tag{2}$$

where δ_{ij} is the Kronecker delta. According to the Stokes Einstein model [16], D_t is defined as:

$$D_t = \frac{K_B T}{3\pi\eta\sigma}. \tag{3}$$

We have approached the electrostatic force between particles i, j by using the Yukawa potential [17]

$$V^Y(r_{ij}) = V_0\frac{e^{-k(r_{ij}-\sigma)}}{r_{ij}}, \tag{4}$$

where r_{ij} the distance between the i and j particles, k^{-1} is the Debye screening length, V_0 is a constant parameter. In our model V_0 Will be modeled with experimentally zeta potential values of MN, as we will see later.

The particle-wall (mica) interaction is approached by the potential derived from the Debye Huckel theory (18)

$$\Phi\,(z_i) = \frac{2\pi\sigma_w}{k\epsilon}\exp\left(k\,(\sigma - z_i)\right), \tag{5}$$

where z_i is the distance from the wall to the i particle, σ_w is the charge density of the wall surface and $\epsilon = K\epsilon_0$ is the dielectric permittivity of the aqueous suspension, K is the dielectric constant (assumed as 80) and ϵ_0 is the vacuum electric permittivity.

The magnetic dipole rotational movement is obtained similarly through the equation [15]

$$\Omega_i\,(t+\Delta t) = \Omega_i\,(t) + \frac{D_r\Delta t}{K_B T}\,(\Gamma_{ij}) + \omega_i(\Delta t), \tag{6}$$

where $\Omega_i\,(t)$ is the rotation vector of the dipole moment at time t, D_r is the rotational difusion coefficient at infinite dilution of the particles, Γ_{ij} is the torque of particle i due to the influence of particle j with dipole moment μ_i. Finally, $\omega_i(\Delta t)$ is the random rotation vector with zero average and covariance.

$$< \omega_i\,(\Delta t)\,\omega_j\,(0) \geq 2D_r\Delta t\delta_{ij}, \tag{7}$$

where, similarly as the translational case, D_r is given by the Stokes-Einstein relationship.

$$D_r = \frac{2K_B T}{\pi\eta\sigma^3}, \tag{8}$$

The dipole-dipole interaction for the i and j particles is given by the relationship:

$$F_{ij} = \frac{3\mu_0\mu^2}{r_{ij}^4},\Big[\cos(\epsilon_{ij}) - 5\cos(\theta_i)\cos(\theta_j)\left(\frac{r_{ij}}{r_{ij}}\right) + \cos(\theta_j)u_i + \cos(\theta_i)u_j\Big], \tag{9}$$

where ε_{ij} is the angle between the unitary vectors u_i and u_j, θ_i and θ_j are the angles between the vector r_{ij} and the unit vectors u_i and u_j, respectively.

The torque between dipoles i and j is given by

$$\Gamma_{ij} = \frac{-\mu_0\mu^2}{r_{ij}^3}\left[u_i \times u_j - 3\cos(\theta_j)\frac{u_i \times r_{ij}}{r_{ij}}\right],$$
$$\Gamma_{ji} = \frac{-\mu_0\mu^2}{r_{ij}^3}\left[u_j \times u_i - 3\cos(\theta_i)\frac{u_j \times r_{ij}}{r_{ij}}\right], \tag{10}$$

We also investigate the influence of van der Waals forces between particles and the interaction with a plane surface [6]:

$$\overrightarrow{F}_{ij}^{VDW} = \frac{-A_{ij}}{3a}\left(\frac{2r_{ij}}{\left(r_{ij}^2-4\right)^2} + \frac{2}{r_{ij}^3} - \frac{r_{ij}}{\left(r_{ij}^2-4\right)} + \frac{1}{r_{ij}}\right) \times \frac{\overrightarrow{r}_{ij}}{r_{ij}}, \overrightarrow{F}_{iw}^{VDW} = \frac{A_{iw}}{6a}\left(\frac{1}{\delta_{iw}^2} + \frac{1}{(\delta_{iw}+2)^2} - \frac{1}{\delta_{iw}} + \frac{1}{(\delta_{iw}+2)}\right)\widehat{k}, \tag{11}$$

where $\overrightarrow{F}_{ij}^{VDW}$ is the van der Waals force between i and j particles and $\overrightarrow{F}_{iw}^{VDW}$ is the force between particle i and the surface (w); r_{ij} is the interparticle distance between particles respect to the radius of the particles a, δ_{iw} is the surface to particle surface distance, $\widehat{k}$ is the unitary vector in the z direction; A_{ij} and A_{iw} are the Hamaker constants for the $i-j$ particles interaction and the $i-w$ interaction, respectively.

The average magnetic dipole magnetization is obtained for a spherical volume L^3.

$$M = \frac{4\pi}{3(L)^3}\sum_{i=1}^{N} i. \tag{12}$$

The orientational behavior of magnetic nanoparticles was investigated by the use of the orientational order parameter [19]

$$S = \frac{3}{2}\left\langle\cos(\beta)^2\right\rangle - \frac{1}{2}, \tag{13}$$

where β is the angle between the direction of the magnetic dipole moment and the preferred direction (the director), taken as the laboratory z axis. The parenthesis means average of the total magnetic dipoles of the sample. In two dimensions we use the orientational parameter

$$s = 2\langle\cos(\emptyset)^2\rangle - 1, \tag{14}$$

where $\emptyset$ is the angle between the direction of the magnetic dipole moment and one of the axes in the plane.

1.2. Parameters of the simulation

Magnetic dipole moments are given for magnetite with an average diameter $\sigma = 10$ nm (most of the cases) with $\mu = 2.5 \times 10^{-19}$ Am^2. At room temperature $T = 300$ K, water viscosity was assumed as $\eta = 0.96 \times 10^{-3}$ Kg/ms, $\sigma_w = z^{'}$, 2.1×10^{14} charges/cm^2 is the surface charge of mica obtained from references [20,21] when $z^{'}$ is taken as 1. The charge of MN was taken as in Ref. [22] from MN covered with chitosan chain molecules in aqueous suspension and was calculated from the Grahame equation [22]. We obtained the surface charge of particles (around 60 electronic charges). Hamaker constants were approached by 2.0×10^{-19} J [6]. The constant V_0 in the Yukawa potential was approached with the relationship: $V_0 = q^2/4\pi\epsilon$, where q is the charge of the particles ($q = z * 1.6 \times 10^{-19}$ C) and z represents the number of charges at the surface of magnetic particles. The maximum concentration of particles used was 0.01 σ^3 and the maximum number of particles used was 787. Time step was taken as a fraction of 10^{-9} s and 1.5×10^6 steps were employed. Structure in three and two dimensions was analyzed with the radial distribution function [6].

The simulation box was centered at the coordinate origin ($-L/2 < x < L/2$; $-L/2 < y < L/2$; $-L/2 < z < L/2$ Periodic boundary conditions were used for the x and y directions and the wall was set at $z = -L/2$.

We simplify Eqs. (1) and (6) by using a nondimensional length unit r' ($r = r'\sigma m$) and nondimensional time t' ($t = t' 1 \times 10^{-9}$ s)

The equations are rewritten as:

$$\mathbf{r'_i}(t' + \Delta t') = r'_i(t') + A\Delta t' \left(B \sum_{j=1}^{N} \left[\cos(\epsilon_{ij}) - 5\cos(\theta_i)\cos(\theta_j) \left(\frac{\mathbf{r'_{ij}}}{r'_{ij}} \right) + \cos(\theta_j)\mathbf{u_i} + \cos(\theta_i)\mathbf{u_j} \right] \right)$$

$$+ C\frac{1}{(r'^2_{ij})}(1 + kr'_{ij})\hat{r}'_{ij} + \mathbf{Dexp}(k\sigma(1 - z'_i)) + \mathbf{E} * \mathbf{R'_i}(\Delta t')\sqrt{\Delta t'}. \quad (15)$$

Similarly for the rotational displacement

$$\Omega_i(t' + \Delta t') = \Omega_i(t') + F\Delta t' \times \left(G \left[u_i \times u_j - 3\cos(\theta_j)\frac{u_i \times r'_{ij}}{r'_{ij}} \right] \right) + H\omega'_i(\Delta t')\sqrt{\Delta t'}. \quad (16)$$

Parameters A, B, C, D, F and G are obtained from Eqs. (1) and (6), E and H are parameters derived from Eqs. (2) and (7). $R'_i(\Delta t')$ and $\omega'_i(\Delta t')$ are gaussian random numbers, generated for each particle and time of the simulation.

2. Results and discussion

2.1. Charged MN interacting with a charged wall

We first compare the results of the deposition process of charged MNs with a diameter of 26 nm and a magnetic moment of hematite 6×10^{-21} J/T, as obtained by Morga *et al.* [11]. From the values of zeta potential and charge in Ref. [11], we used an average surface charge of MN of Z = 25 electronic charges ($C = 0.2$) and considered the van der Walls interactions [11]. In Fig. 1a) and b) we show the results obtained by Morga *et al.* [11], using hematite MNs with an average diameter of 26 nm.

TABLE I. Simulation results of charged MNP interacting with a charged wall.

Simulation $N = 787$	Parameter C	Parameter D	Box size (σ^3)	Average Separation (σ)	Proportion of particles at the surface (%)
1	4	10	$42 \times 42 \times 42$	1.8	84
2	5	5		2.3	43
3	1	5		No order	100
4	0.1	1		No order	99
5	0.1	1	$60 \times 60 \times 60$	No order	75
6	1	0.1		5.8	17
7	1	1		2.8	69
8	5	1		4.6	24
9	5	10		2.4	100
10	5	100		2.4	100

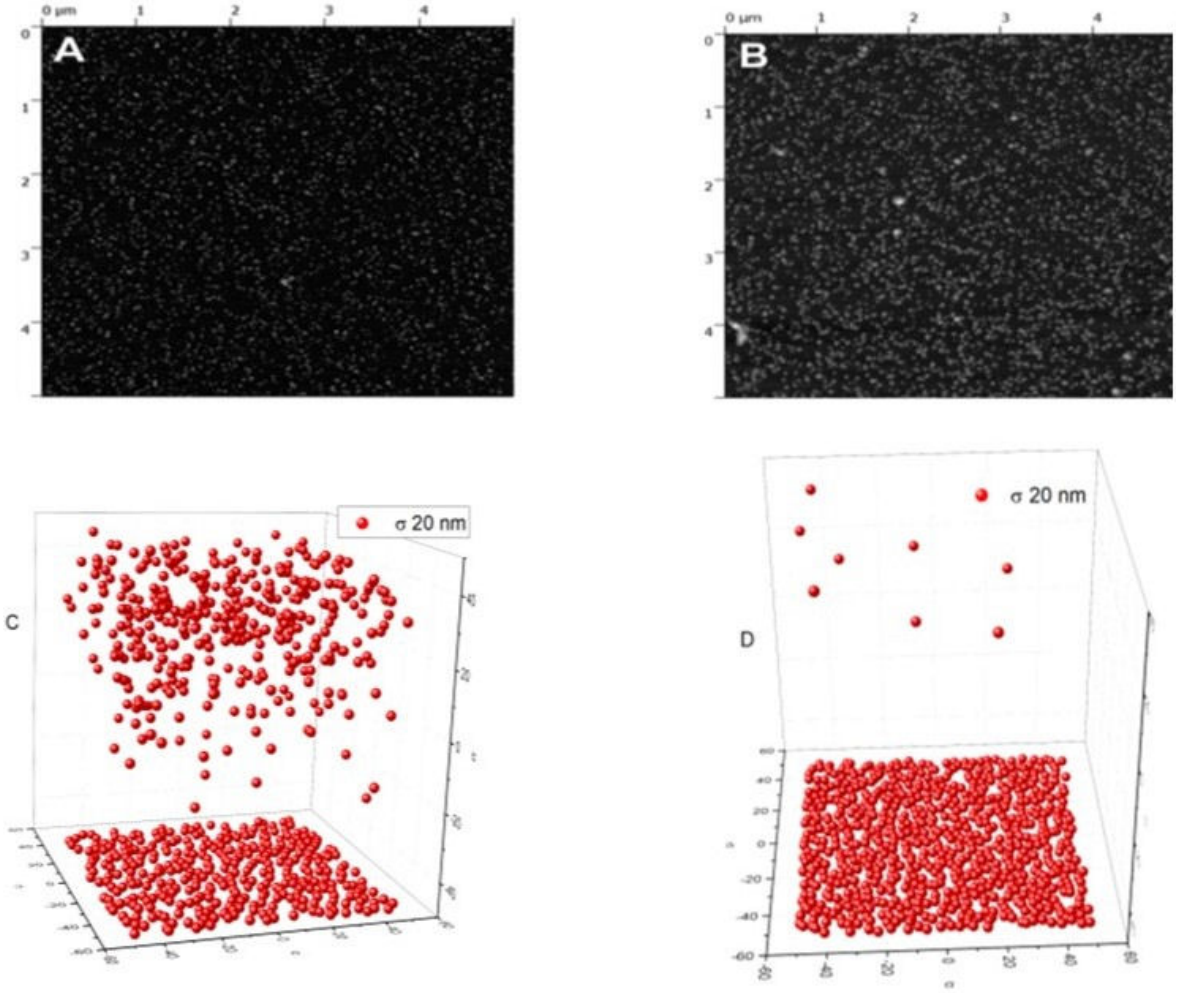

FIGURE 1. a) Liquid phase AFM image of the hematite nanoparticle monolayer obtained for particle deposition conditions: bulk concentration = 50 mg/l, pH 5.8, $T = 298$ K and the deposition time $t = 4$ min, particles concentration = 117 particles μ^{-2} and b) $t = 7$ min, with particles concentration = 163 particles μ^{-2}. Reprinted with permission from Ref. [11]. Copyright 2018 Royal Society of Chemistry. c) B D simulation of deposition of charged MN on a solid surface with surface charge of $\sigma_w = 2.1 \times 10^{14}$ charges/cm^2 and 90 particles μ^{-2} at 0.1 s d) deposition time of 0.2 s and 180 particles μ^{-2} at the surface.

In Fig. 1a), we observe short chains of MNs due to the magnetic dipole attraction, probably due to the low magnetic moment of hematite. It is also possible that the small surface charge on MNs, prevented the formation of ordered arrays of MN on the surface. Similar results are depicted in Fig. 1b), albeit with a higher amount of MNs deposited on the surface. In Fig. 1c) and 1d) show comparable behavior observed in our simulation. However, MNs deposited on a mica-like surface were achieved in shorter times.

On the other hand, ordered MN have been obtained by some researchers [9,10] using the Langmuir-Blodgett technique. In Fig. 2 we observe TEM and a AFM images of MNs in a hexagonal array structure. Most of the methods used by these authors to achieve ordered magnetic nanoparticles arrays involve the use of polymers, surfactants, or other molecules to stabilize two dimensional magnetic nanoparticles arrays. This suggests that the presence of the molecules on the surface of MNs contributes to the stability of the particle arrangement on the surface. In this regard, we conducted different Brownian dynamic simulations with charged nanoparticles and interacting with a charged surface, simulating charged mica Eq. (5).

Our results show the behavior of various charged MNs and different surface charge (Fig. 3). When using MNs with low charge parameter $C = 0.1$ and a surface charge density parameter $D = 1$ for the solid surface, we observe that after a simulation time of 15 μs, most of the particles (75 % of all particles) reach the surface. However, they do not form ordered arrangements; instead, they assemble into short chains of particles [Fig. 3a)]. This behavior is similar to the one described above in Fig. 1. By increasing the surface charge of MN $C = 1$ and decreasing the charge density of the plane surface $D = 0.1$, we observe a more ordered array at the surface with an average particle separation of 5.8 σ [Fig. 3b)]. However, the proportion of particles at the surface is lower (17 %). In this case, magnetic dipole attraction between particles does not seem to be strong enough to form chains. With the same surface charge of MNs $C = 1$ and an increase in the

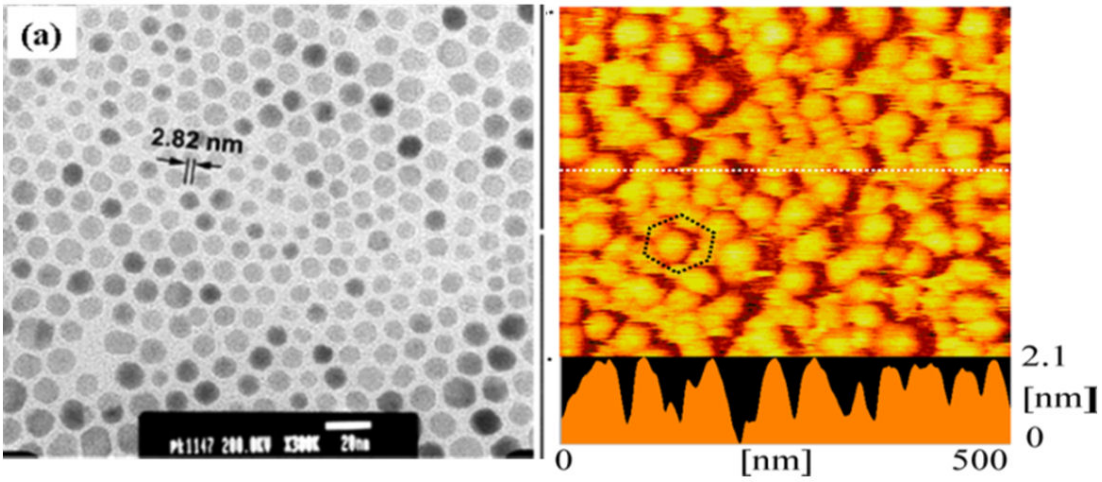

FIGURE 2. a) TEM image of 10 nm magnetite nanoparticles. Reprinted with permission from ref. [9]. Copyright 2007 American Chemical Society. b) AFM image of single-particle layer of organo-modified $CoFe_2O_4$ fabricated by "repeating compression-expansion method". Reprinted with permission from Ref. [10]. Copyright 2015 American Chemical Society.

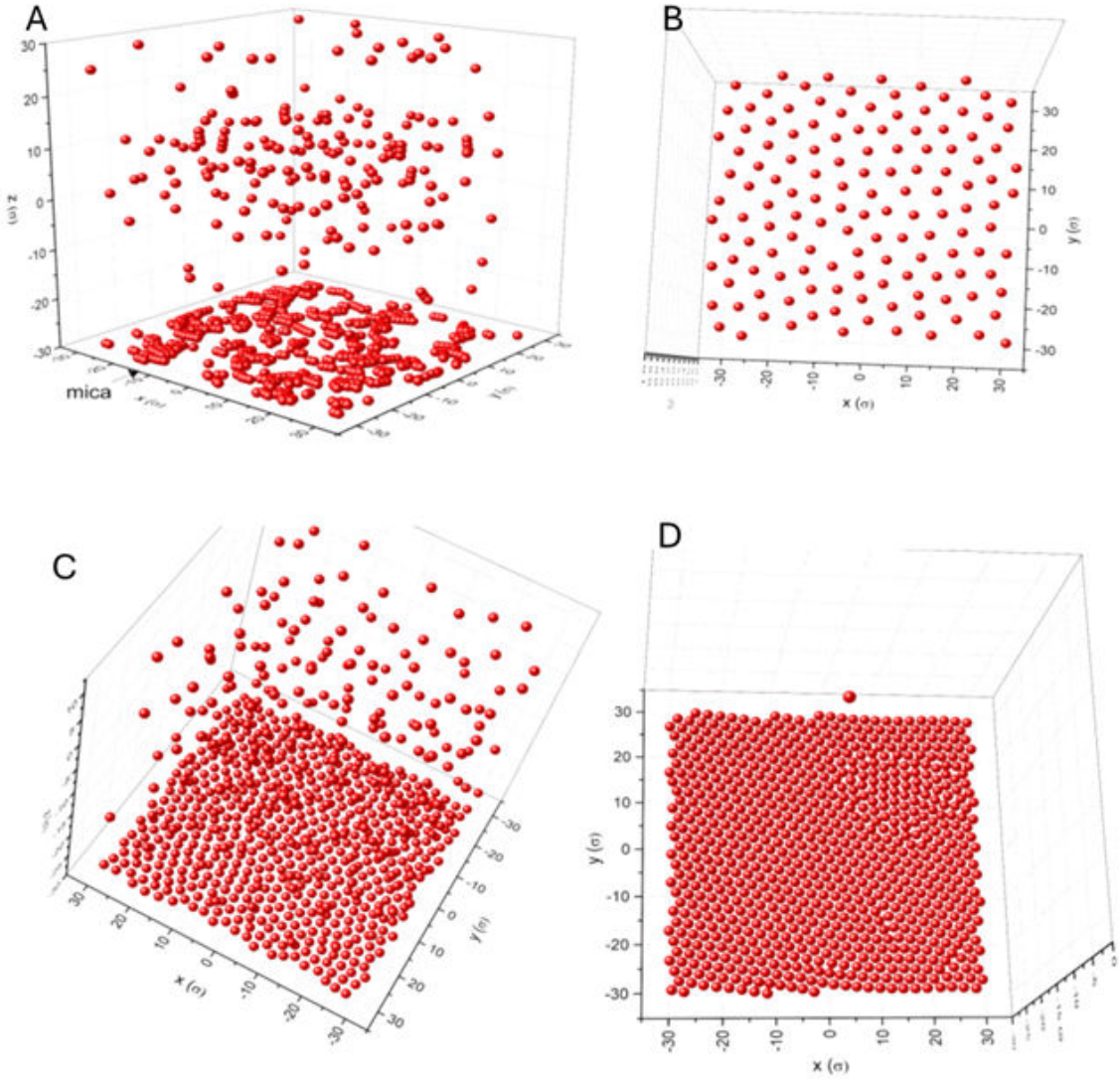

FIGURE 3. a) MN with charge parameter $C = 0.1$ ($z = 18$) and surface charge parameter $D = 1$, b) $C = 1$ and $D = 0.1$, c) $C = 1$ and $D = 1$, d) $C = 5$ and $D = 10$.

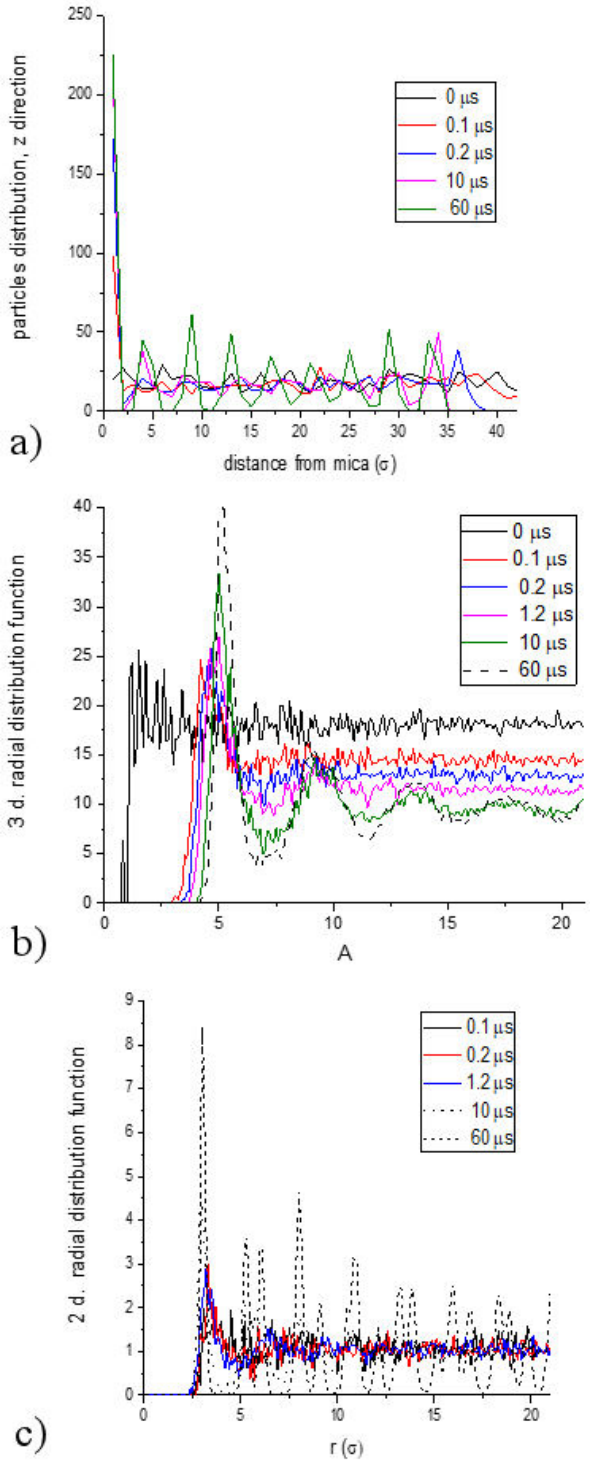

FIGURE 4. Time behavior of a system of 784 MN in a $42 \times 42 \times 42\sigma^3$ simulation box. A charge parameter of $C = 2$, a magnetic dipolar moment of 1.25×10^{-19} Am^2, and diameter $\sigma = 10$ nm. a) Vertical profile of particles at different times. b) Radial distribution function in the bulk at different times. c) Time behavior of two-dimensional distribution function of MN on the surface, simulating mica.

charge density at the surface $D = 1$, more particles are deposited at the surface (70 %), with an average separation of 2.8 σ [Fig. 3c)]. This indicates that the intensity of electric repulsion among particles plays a crucial role in forming ordered structures at the surface, and a higher attraction to the surface increases the number of particles at the surface. Figure 3d) shows an ordered system using $C = 5$ and higher charged surface parameter $D = 10$, resulting in an almost hexagonal ordered particles array with an average separation of 2.4 σ. In this case, practically all charged MNs are attracted at the surface.

Additionally, the orientational order parameter was measured for simulations. Figure 3a) showed a small orientation along the x axis of MN on the solid surface. This occurred spontaneously, probably, as soon as particles arrived at the surface and to the small electric repulsion. From Eq. (14), we obtained a s value of 0.28, very close to the lower limit of an ordered liquid crystal. On the other hand, from Eq. (12) we obtained the average dipole moment $\mu = 2.5 \times 10^{-19}$ Am^2 ($\vec{\mu} = 0.287\hat{\imath} - 0.018\hat{\jmath} - 0.02\hat{k}$) which corroborates a small orientation of particles along x axis. The orientational parameter of the simulation S calculated shown in Fig. 3b) B was also small (0.27) but in direction perpendicular to the surface. On the contrary, simulations shown in Figs. 3c) and 3d) did not show any preferred orientation.

Table I shows simulation results obtained using various surface charge of MNs and different charge density on the bottom surface of the box. Two box sizes were used $42 \times 42 \times 42\sigma^3$ and $60 \times 60 \times 60\sigma^3$. We assumed van der Walls, magnetic, electric, and Brownian interactions between particles.

We noticed that when using a small charge parameter $C = 0.1$ on the surface MNs, these are deposited on the surface $D = 1$ in non-ordered arrays for both concentrations used. However, in the smaller box, almost all particles are attracted to the surface. These results resemble those observed in Fig. 1 for experimental results, where magnetic interactions dominate. On the other hand, by increasing the charge of MNs $C = 1$ and using $D = 0.1$ at the surface with a box size of $60 \times 60 \times 60\sigma^3$, we obtain a more ordered structure and a higher proportion of particles 69% reached surface $D = 1$. It is interesting to observe that for the same charge on the MNs $C = 1$ and a higher plane surface charge $D = 5$ and smaller box (case 3), all particles are attracted at the surface but are not ordered. This suggests that particles are strongly attracted to the surface and do not have enough freedom to move in the xy plane to achieve ordering.

Now, we compare the results using more charged particles $C = 5$ and a plane surface chargeparameter $D = 1$, 10 and 100 (lines 8, 9, and 10 in Table I). We observed that for $D = 1$, only 24% of particles are attracted at the plane surface and the average particle separation is 4.6 σ. Increasing the attraction with the surface ($D = 10$, 100), we observe that all particles are deposited at the surface, forming an almost perfect two-dimensional hexagonal structure with particle-particle separation of 2.4 σ. The cases (lines 1 and 2 in the table) show that for a more concentrated particle system, the increase of the plane surface charge is not sufficient to admit all particles at the surface to the, even with a surface

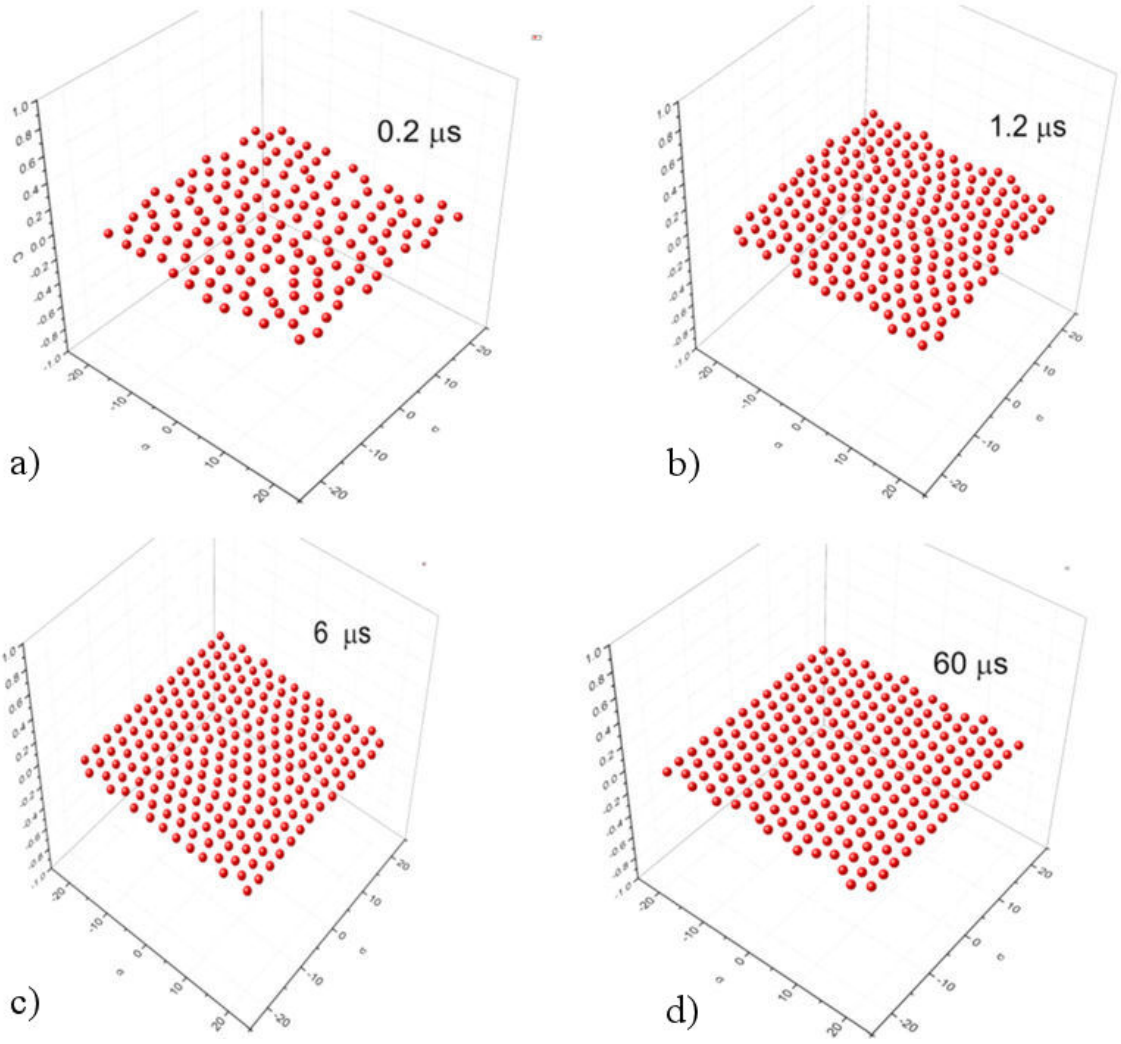

FIGURE 5. Two-dimensional structure of MN on the solid surface at different times with the parameters given in Fig. 4 produced in the deposition process of charged MN on a mica like surface. a) 98 particles at the surface after 0.2 μs, b) 172 particles after 1.2 μs, c) 219 particles after 6 μs and d) 225 particles after 60 μs.

charge parameter of MN of $C = 4$ and $C = 5$. This is probably due to a charged repulsive barrier formed by particles at the plane surface. However, particles remain ordered at the surface with a smaller separation (1.8σ and 2.3σ).

Finally, we analyze the behavior of MNs interacting with a charged wall at different times. We use a particle concentration of 0.01 Particles/σ^3 and a simulation box of $42 \times 42 \times 42\sigma^3$. In Fig. 4a), we show the time behavior of the particles profile at different distances from the charged surface. We observe that, as time increases, 20, 98, 172, 219 and 225 particles arrive at the surface at 0, 0.1, 0.2, 10 60 μs, respectively. After this time, no more particles arrive at the surface due to the electrostatic barrier formed on the charged surface. Additionally, notice that after 10 μs, particles form some kind of stratified zones, where MNs are aggregated in about 8 planes separated approximately by 4 σ and remain stable.

Figure 4b) shows the behavior of the radial distribution function of the particles (6) in the box, (excluding the particles on the surface), at different times. In order to show differences in the distributions, the graphs were not normalized. As expected, initially, despite using only one configuration, particles show a uniform and random distribution. At 0.1 μs, it is observed a first peak at 4σ. This first peak is shifts to approximately 5σ at 60 μs, this is probably due to the final position of particles, which is closer to the solid surface, with fewer particles remaining in the bulk. Additionally, we observe that at this time, the remaining particles in the bulk (about 70%) form a relatively ordered structure. The behavior of MNs at the solid charged surface is shown in Fig. 4c). Two-dimensional distribution functions are shown for different times after the simulation started. We observe that at 60 μs, MNs show a hexagonal structure with about 3σ closest particles distance. After this time, the structure remains stable on the solid surface. This arrangement resembles the findings of some experimental researchers [9,10], as explained earlier.

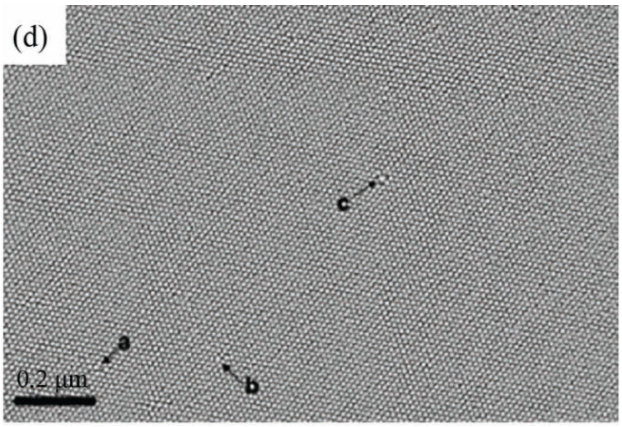

FIGURE 6. Background SEM image of 11 nm $Fe_xO/CoFe_2O_4$ MN on a Pt-covered Si substrate by tape-casting method. Reprinted with permission from Ref. [26]. Copyright 2012 Wiley-VCH Verlag GmbH & Co. KGaA, Weinheim.

In Fig. 5 we show the structure of MN on the charged surface at different times after the simulation started with 784 particles with a surface charge of +80e, magnetic dipole moment of 1.25×10^{-19} Am^2 and diameter $\sigma = 10$ nm. After 60 μs we observe a hexagonal arrangement similar to the one found experimentally by some researchers [9,10]. As expected, the orientational order parameter was around 0.

According to experiments performed by different authors with magnetic nanoparticles on surfaces; most of the MNs were stabilized with different molecules which contributed to obtain electric charge at the particle surface [23,24]. In 1999, Lakovenko *et al*. [25] performed Langmuir Blodgett monolayers with stearic acid and found that MNs interacted at the interface with stearic acid molecules trough electrostatic interactions and build hexagonal structures. They mentioned that organic molecules on the MN surface make particles more labile as compared with naked MN. On the contrary, anisotropy and magnetic interactions produce deviations on the 2D array of nanoparticles. Li *et al*. [23] also found hexagonal structures with superparamagnetic iron oxide nanoparticles surrounded by a bilayer of oleic acid 8 nm MN in hexane. Bellido *et al*., [26] demonstrated that phospholipids at the MN surface provide the necessary binding force to hold them tied to the surface forming hexagonal superlattices over extended areas up to 2×2 cm. In Fig. 6 we show a SEM image obtained by Bellido *et al*. [26].

In this regard, we conducted Brownian dynamics simulations in two dimensions of MN with and without charge and taking into account the Van der Walls interaction between particles given by Eq. (11). We used a simulation area of $42\sigma \times 42\sigma$ with 784 particles, each possessing a magnetic dipole moment of $\mu = 2.5 \times 10^{-19}$ Am^2, and varied the parameter of the electric interaction C from 0 to 5.

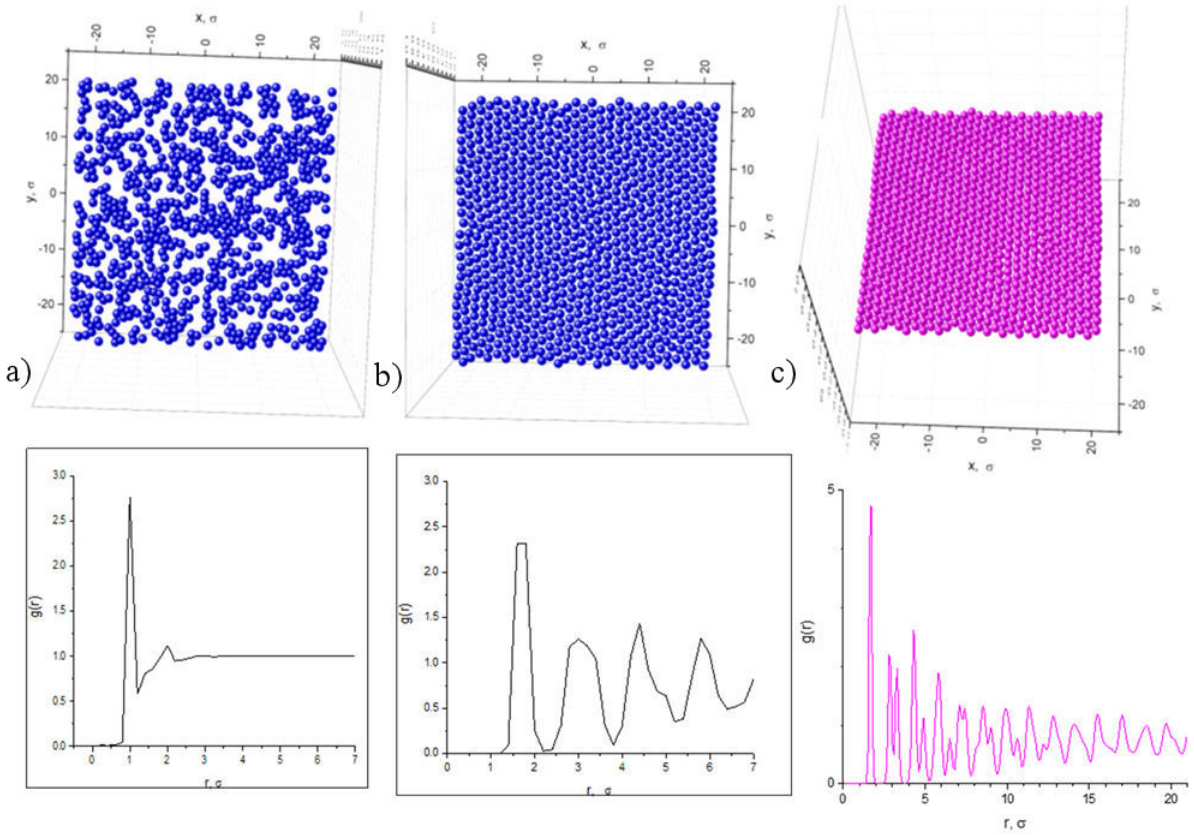

FIGURE 7. Structure of particles and two-dimensional radial distribution function. a) $C = 0$ and $\mu = 2.5 \times 10^{-19}$ Am^2, b) $C = 1$ and $\mu = (1/2) \times 2.5 \times 10^{-19}$ Am^2, c) $C = 2$ and $\mu = (1/2) \times 2.5 \times 10^{-19}$ Am^2.

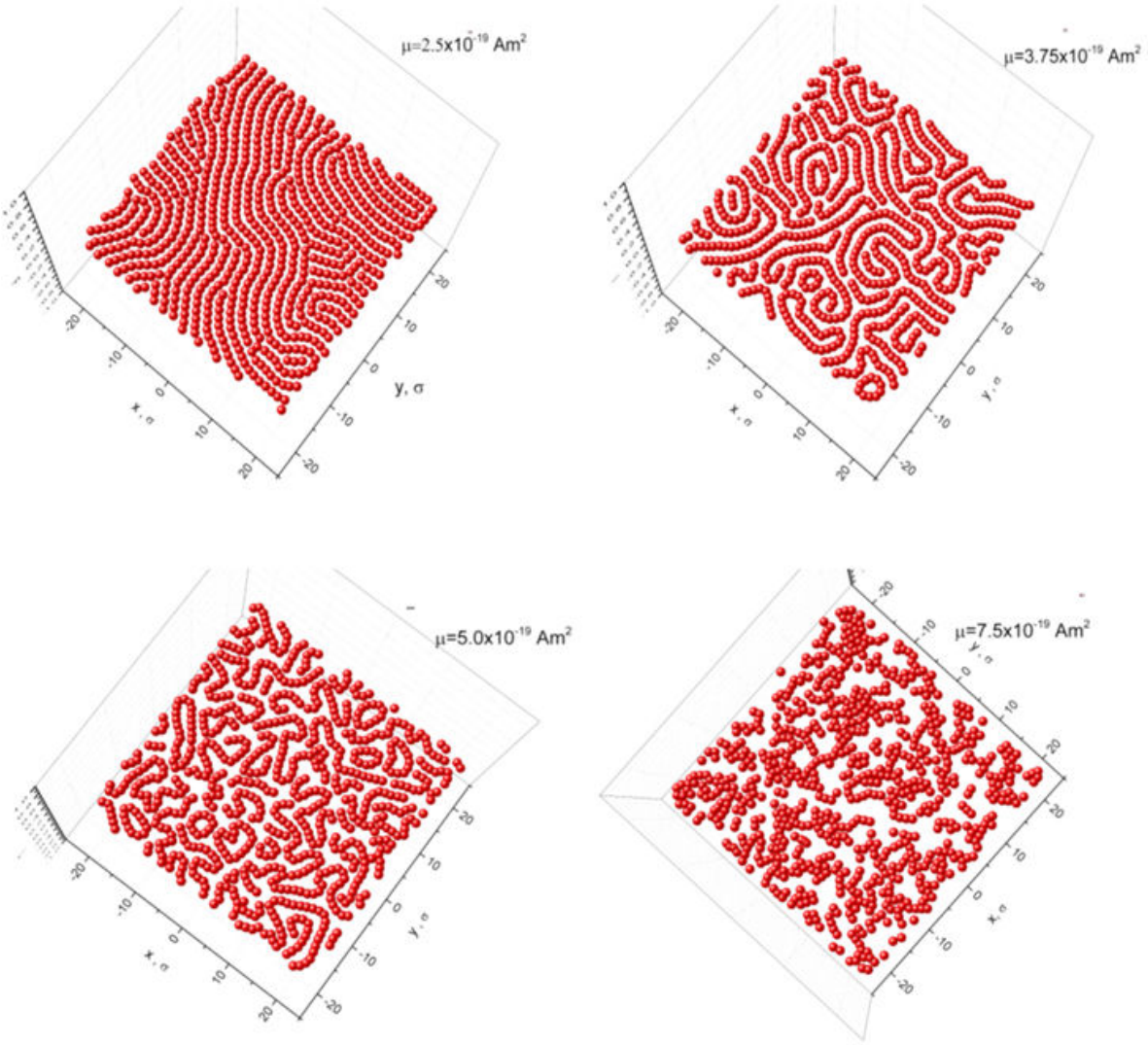

FIGURE 8. Two-dimensional arrays of 784 charged MN with $C = 2$ (80 electron surface charges) and different magnetic dipole moments. a) $\mu = 2.5 \times 10^{-19}$ Am^2, b) $\mu = 3.5 \times 10^{-19}$ Am^2, c) $\mu = 5.0 \times 10^{-19}$ Am^2, d) $\mu = 7.5 \times 10^{-19}$ Am^2.

In Fig. 7a) shows, a disordered and aggregated arrangement of particles is observed for no charged MN. For $C = 1$ (corresponding to 60 charges/particle) and $\mu = \frac{1}{2}2.5 \times 10^{-19}$ Am^2, particles being separated, and form ordered systems [Fig. 7b)]. It is at $C = 2$ when a perfect ordered system is observed [(Fig. 7c)]. This indicates that when particles with the half of the magnitude of magnetic dipole moment are used, ordering arrays of MNs are observed at the surface, when MN with aproximately 80 surface charges/particle are simulated.

We have performed simulations with different magnitude of magnetic dipole moments, keeping constant the surface charge on MN ($C = 2$). Different structures were found at different times. However, the structures were stabilized after 60 μs. In Fig. 8a), we show long chains of magnetic dipoles produced with a dipole magnitude of 2.5×10^{-19} Am^2. The dipole moment of the whole particle system was determined using Eq. (12), resulting in an average value close to zero. Similarly, the orientational parameter s also averaged to zero.

In Fig. 8b), we observed the formation of open and closed chains using $\mu = 3.75 \times 10^{-19}$ Am^2. This behavior is also similar to the one observed by Ghazali and Lévi [27], using Monte Carlo simulations and found experimentally by Benkowski *et al*. [28]. A higher value of the dipole moment, such as 5.0×10^{-19} Am^2 (twice the value for magnetite), results in the formation of disordered small chains and loops, as shown in Fig. 8 C. This behavior resembles that observed by Klokkenburg *et al*. [14], who obtained results using MC simulations with cobalt MN of 15 nm.

Finally, Fig. 8d) shows the disordered aggregation of MNs without chains or loops, produced with the use of a magnetic dipole of $\mu = 7.5 \times 10^{-19}$ Am^2. In this case the dipole-dipole interaction is very strong compared with the electrostatic repulsion among particles, avoiding the formation of ordered structures or chains. In all simulations, the orientational order parameter s averaged approximately zero.

3. Conclusion

In this work, we have used Brownian Dynamics simulations of charged magnetic nanoparticles in three and two dimensions. We simulated the deposition process of particles on charged surfaces, considering dipole-dipole, electrostatic and van de Walls interactions. Our results confirm that electric charges on the surface of magnetic nanoparticles contribute to the hexagonal arrangement of particles on the surface, consistent with the experimental findings. Additionally, charged surface on MNs contribute to increase the particle concentration on the mica-like surface. When electric repulsion is insufficient to separate magnetic dipoles, chains formation dominates, and disorder is achieved.

Furthermore, simulations of charged magnetic dipoles in two dimensions showed the effect of charge on magnetic particles in obtaining hexagonally ordered structures, which aligns with experimental observations using magnetic nanoparticles covered with stearic acid, oleic acid, and other organic molecules.

Acknowledgments

We appreciate the support and facilities of the Area de Cómputo de Alto Rendimiento de la Universidad de Sonora (ACARUS) to perform all our simulations.

1. A. Arbab *et al.*, Review on Recent Progress in Magnetic Nanoparticles: Synthesis, Characterization, and Diverse Applications, *Frontiers in Chemistry* **13** (2021) Sec. Nanoscience 9-629054, https://doi.org/10.3389/fchem.2021.629054
2. L. Zhiming, J. Ma, J. Ruan and X. Zhuang, Using Positively Charged Magnetic Nanoparticles to Capture Bacteria at Ultralow Concentration, *Nanoscale Research Letters* **14** (2019) 195, https://doi.org/10.1186/s11671-019-3005-z
3. T. Javanbakht, S. Laurent, D. Stanicki, W. Raphael, and J. R. Tavares, Charge effect of superparamagnetic iron oxide nanoparticles on their surface functionalization by photo-initiated chemical vapour deposition, *Journal of Nanoparticle Research* **17** (2015) 462, https://doi.org/10.1007/s11051-015-3276-y
4. Y. Wang, P. Li and L. Kong, Chitosan-modified PLGA nanoparticles with versatile surface for improved drug delivery, *American Association of Pharmaceutical Scientists* **14** (2013) 585, https://doi.org/10.1208/s12249-013-9943-3
5. S. Joly *et al.*, Multilayer nanoreactors for metallic and semiconducting particles, *Langmuir* **16** (2000) 1354, https://pubs.acs.org/doi/10.1021/la991089t
6. P. Kulkarni and P. Biswas, A Brownian Dynamics Simulation to Predict Morphology of Nanoparticle Deposits in the Presence of Interparticle Interactions, *Aerosol Science and Technology* **38** (2004) 541, https://doi.org/10.1080/02786820490466747
7. G. Binasch, P. Grunberg, F. Saurenbach and W. Zinn, Enhanced magnetoresistance in layered magnetic structures with antiferromagnetic interlayer exchange, *Physical Review B: Condensed Matter and Materials Physics* **39** (1989) 4828, https://doi.org/10.1103/PhysRevB.39.4828
8. D. M. Eigler, A. J. Heinrich, S. Loth, and C. P. Lutz, Antiferromagnetic storage device, *United States Patent* (2014) No. US8,724,376 B2,
9. D. K. Lee, Y.H. Kim, C. W. Kim, H. G. Cha, and Y. S. Kang, Vast Magnetic Monolayer Film with Surfactant-Stabilized Fe3O4 Nanoparticles Using Langmuir-Blodgett Technique, *Journal of Physical Chemistry B* **111** (2007) 9288, https://doi.org/10.1021/jp072612c
10. A. Fujimori, K. Ohmura, N. Honda, and K. Kakizaki, Creation of High-Density and Low-Defect Single-Layer Film of Magnetic Nanoparticles by the Method of Interfacial Molecular Films, *Langmuir* **31** (2015) 3254, https://doi.org/10.1021/acs.langmuir5b00241
11. M. Morga, Z. Adamczyk, D. Kosior and M. Oćwieja, Hematite/silica nanoparticle bilayers on mica: AFM and electrokinetic characterization, *Physical Chemistry Chemical Physics* **20** (2018) 15368, https://doi.org/10.1039/C8CP01049H
12. M. Tadic, M. Panjan, V. Damnjanovic, and I. Milosevic, Magnetic properties of hematite (α-Fe2O3) nanoparticles prepared by hydrothermal synthesis method, *Applied Surface Science* 320 (2014) 183, https://doi.org/10.1016/j.apsusc.2014.08.193
13. M. H. D. M. Rodrigues, J. B. Souza Junior, and E. R. Leite, The Influence of Magnetic Field and Nanoparticle Concentration on the Thin Film Colloidal Deposition Process of Magnetic Nanoparticles: The Search for High-Efficiency Hematite Photoanodes, *Nanomaterials* **12** (2022) 1636, https://doi.org/10.3390/nano12101636
14. M. Klokkenburg, C. Vonk, E. M. Claesson, J. D. Meeldijk, B. H. Ernè and A. P. Philipse, Direct Imaging of Zero-Field Dipolar Structures in Colloidal Dispersions of Synthetic Magnetite, *Journal of the American Chemical Society* **126** (2004) 16706, https://doi.org/10.1021/ja0456252
15. M.E. Cano *et al.*, Magnetisation of red blood cells: a Brownian Dynamics Simulation, *Rev. Mex. Fis.* **58** (2012) 391, https://www.scielo.org.mx/scielo.php?script=sci_arttext&pid=S0035-001X2012000500004
16. D. L. Ermak and J. A. McCammon, Brownian dynamics with hydrodynamic interactions, *Journal of Chemical Physics* **69** (1978) 1352, https://doi.org/10.1039/CS9851400421
17. W.-K. Qi, Z. Wang, Y. Han, Y. Chen, Melting in two-dimensional Yukawa systems: A Brownian dynamics simulation, *Journal of Chemical Physics* **133** (2010) 234508, https://doi.org/10.1063/1.3506875.

18. E. Bianchi, C. N. Likos, and G. Kahl, Self-assembly of heterogeneously charged particles under confinement, *ACS Nano* **7** (2013) 4657, https://doi.org/10.1021/nn401487m

19. C. Zannoni, Order parameters and orientational distributions in liquid crystals, en *Polarized Spectroscopy of Ordered Systems*, eds. B. Samorì y E. Thulstrup, Kluwer (1988), pp. 57-83, https://doi.org/10.1007/978-94-009-3039-1

20. P. M. Claesson, P. Herder, P. Stenius, J. C. Ericksson, and R. M. Pashley, An ESCA and AES study of ion-exchange on the basal plane of mica, *Journal of Colloid and Interface Science* **109** (1986) 31, https://doi.org/10.1016/0021-9797(86)90278-X.

21. B. L. Dixon Northern, Y. L. Chen, J. N. Israelachvili, and J. A. N. Zasadzinski, Atomic force microscopy of mica surface after ion replacement, *Proceedings of the 49th Annual Meeting of the Electron Microscopy Society of America* **49** (1991) 628, https://doi.org/10.1038/s41467-023-35872-y.

22. J. Ibarra *et al.*, Synthesis and characterization of magnetite/PLGA/chitosan nanoparticles, *Mater. Res. Express* **2** (2015) 095010, https://dx.doi.org/10.1088/2053-1591/2/9/095010.

23. D. Liu, J. Wu, C. Kim and J. D. Fortner, Aqueous Aggregation and Surface Deposition Processes of Engineered Superparamagnetic Iron Oxide Nanoparticles for Environmental Applications, *Environ. Sci. Technol.* **48** (2014) 11892, https://doi.org/10.1021/es502174p.

24. Yu *et al.*, Surface Modification of Magnetic Iron Oxide Nanoparticles, *Nanomaterials* **8** (2018) 810, http://dx.doi.org/10.3390/nano8100810,

25. S. A. Iakovenko *et al.*, One- and Two-Dimensional Arrays of Magnetic Nanoparticles by the Langmuir-Blodgett Technique, *Adv. Mater.* **11** (1999) 388, https://doi.org/10.1002/(SICI)1521-4095(199903)11:5

26. E. Bellido, N. Domingo, I. O. Jiménez and D. Ruiz-Molina, Structuration and Integration of Magnetic Nanoparticles on Surfaces and Devices, *small* **8** (2012) 1465, https://doi.org/10.1002/smll.201101456

27. A. Ghazali and J. C. Lévy, Two-dimensional arrangements of magnetic nanoparticles, *Phys. Rev. B* **67** (2003) 064409, https://doi.org/10.1103/PhysRevB.67.064409

28. J. J. Benkowski *et al.*, Self-Assembly of Polymer-Coated Ferromagnetic Nanoparticles into Mesoscopic Polymer Chains, *Journal of Polymer Science: Part B: Polymer Physics* **46** (2008) 2267, https://doi.org/10.1002/polb.21558